Thermal Oxidation and Unwrinkling of Chemical Vapor Deposition–Grown Graphene

ARTICLE *in* THE JOURNAL OF PHYSICAL CHEMISTRY C · SEPTEMBER 2012

Impact Factor: 4.77 · DOI: 10.1021/jp306537y

3 AUTHORS:

Sumedh Surwade
Fujifilm Imaging Colorants Inc
43 PUBLICATIONS **997** CITATIONS
SEE PROFILE

Zhiting Li
University of Pittsburgh
12 PUBLICATIONS **218** CITATIONS
SEE PROFILE

Haitao Liu
University of Pittsburgh
47 PUBLICATIONS **1,952** CITATIONS
SEE PROFILE

THE JOURNAL OF PHYSICAL CHEMISTRY C

Article

pubs.acs.org/JPCC

Thermal Oxidation and Unwrinkling of Chemical Vapor Deposition-Grown Graphene

Sumedh P. Surwade, Zhiting Li, and Haitao Liu*

Department of Chemistry, University of Pittsburgh, Pittsburgh, Pennsylvania 15260, United States

Supporting Information

ABSTRACT: We report the atmospheric thermal oxidation of chemical vapor deposition (CVD)-grown graphene and its effect on the wrinkles in graphene. Heating CVD-grown single-layer graphene in air at 550 °C leads to the disappearance of the wrinkles and the formation of nanoscale cracks and pits in the basal plane. Under this reaction condition, the wrinkles were not preferentially attacked by O_2, which we attribute to the relaxation of wrinkles as well as the presence of more reactive point defects and grain boundaries in the basal plane. Randomly stacked two-layer graphene was found to be more stable toward oxidation than was single-layer graphene.

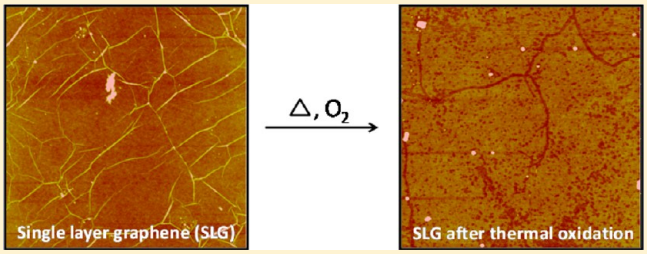

INTRODUCTION

The interesting properties of graphene have attracted researchers from different fields of science and lead to its use in a wide range of applications such as electronics, optoelectronics, energy storage, and sensors.[1−8] Among the several approaches for synthesizing graphene, the chemical vapor deposition (CVD) growth of graphene on copper substrate has the distinct advantage of being able to provide very large graphene films that can be transferred to different substrates.[9−13] Many of the potential applications of graphene will subject it to a very harsh environment. Consequently, understanding the chemical property of graphene is critical to evaluating its long-term stability in these applications.

The thermal oxidation by oxygen limits the high temperature stability of graphene in an oxygenated environment. The thermal oxidation of microexfoliated graphene and graphite is the subject of several recent studies. Liu et al. recently studied the thermal oxidation of exfoliated graphene and observed nanoscale pits and cracks upon oxidation.[14] Similar nanoscale pits were also observed in the ozone oxidation of graphite by several groups.[15−18] The formation of nanoscale pits and cracks on graphene and graphite was attributed to the preferential attack of oxygen on the point defects and grain boundaries in graphene basal plane. Other studies showed that the edge of the graphene has enhanced reactivity as well. For example, Wang et al. used a dilute mixture of O_2/NH_3 to etch graphene at high temperature and observed preferential attack on the edge of graphene.[19]

The above studies indicate that the structural defects play a major role in the oxidative etching of graphitic materials. CVD-grown graphene has three major types of structural imperfections: grain boundaries, point defects, and wrinkles. Among them, grain boundaries and point defects are also commonly found in graphite and exfoliated graphene. Several recent studies have shown that the copper-based CVD-grown graphene is polycrystalline with grains in the range of several to several tens of micrometers.[20−26] The growth of graphene on a copper substrate is not epitaxial; a single crystalline domain of graphene can cross Cu grain boundaries.[27] The atomic structure of grain boundaries in CVD graphene consists of series of pentagons, heptagons, and distorted hexagons.[24,26,28] The presence of point defects in CVD-graphene can be seen in the micro-Raman spectrum of graphene, which showed a weak D peak even in areas free of grain boundaries.[9]

Theoretical studies on graphene grain boundaries show that the inhomogeneous strain field at grain boundaries increases their reactivity.[29] Other theoretical studies found that the oxidative erosion of graphene is faster at the defect site as compared to the nondefect site,[30] and that the zigzag edges of graphene nanoribbons are more reactive as compared to graphene sheet, carbon nanotube, and armchair-edged graphene nanoribbons.[31] These theoretical predictions were consistent with the experimental study on the etching of mechanically exfoliated graphene, which showed that oxygen molecules[14,32] and hydrogen plasma[33] preferentially attack grain boundaries and point defects to produce nanoscale cracks and pits, respectively.

Unlike grain boundaries and point defects, wrinkles are unique in that they are commonly found in CVD-grown graphene but usually not present in graphite and exfoliated graphene. CVD-grown graphene is typically synthesized at ∼1000 °C, and upon cooling to room temperature, wrinkles form in the graphene layer due to the large difference in the thermal expansion coefficient between graphene and the copper

Received: July 2, 2012
Revised: August 29, 2012
Published: August 31, 2012

dx.doi.org/10.1021/jp306537y | J. Phys. Chem. C 2012, 116, 20600−20606

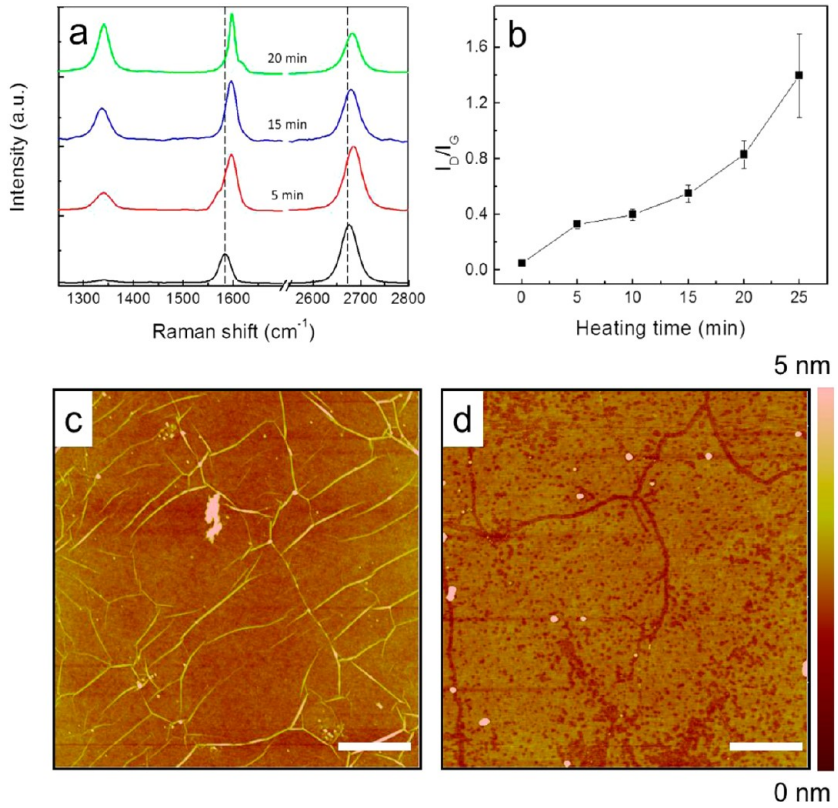

Figure 1. (a) Raman spectra of single-layer graphene on a Si/SiO_2 substrate before (black) and after heating at 550 °C for 5 min (red), 15 min (blue), and 20 min (green). (b) Ratio of the intensity of G mode to D mode (I_D/I_G) as a function of heating time. The error bar is the standard deviation of 10 measurements taken at random locations. AFM images of CVD-grown single-layer graphene on a Si/SiO_2 substrate (c) before and (d) after heating at 550 °C for 20 min in air. Scale bars represent 1 μm. The images were taken at different locations.

substrate. It was also shown that the surface roughness of copper substrate contributes to the formation of wrinkle upon transferring graphene to a flat substrate.[34] The wrinkle is made of locally folded graphene film.[35] Because of the high local curvature, such folded graphene may show enhanced reactivity toward O_2 oxidation. As an example, the diameter-dependent reactivity in carbon nanotubes was explained in terms of radial strain.[36,37] The enhanced reactivity of wrinkles in exfoliated graphene toward O_2/NH_3 etching was recently reported by Wang et al.[19] In addition, Starodub et al. also observed preferential etching of wrinkles by O_2 on a graphene sample grown on Ir (111).[38] On the other hand, Han et al. observed that steam etching of reduced graphene oxide preferentially occurs on point defects but not on wrinkles.[39] In a recent study, we observed that the UV/O_3 oxidation of a CVD-grown single-layer graphene is a nonselective process that does not preferentially attack existing defects, grain boundaries, or wrinkles.[40] Given the wide range of reactivities observed, it is important to understand if and to what extent the wrinkles affect the oxidation of CVD-grown graphene.

In this study, we report the thermal oxidation of CVD-grown single-layer and randomly stacked two-layer graphene using atmospheric oxygen. Our study aims to understand the effect of oxidation and high temperature treatment on the wrinkles in CVD-grown graphene. Our result shows that graphene unwrinkles itself at high temperature and the oxidation does not preferentially initiate on the wrinkles. We also find that randomly stacked two-layer graphene, made by overlaying two single-layer graphene films, showed significantly improved resistance to oxidation.

RESULTS AND DISCUSSION

Single-layer graphene was synthesized following a copper-catalyzed CVD method using methane as the carbon source.[9] After the CVD growth, the graphene film was transferred onto a silicon wafer that has a 300 nm thick thermal oxide layer using poly methyl methacrylate (PMMA) as the transferring agent.[13] The thermal oxidation of graphene was carried out by heating the graphene sample at 550 °C in an oven under atmospheric oxygen. The heating time was varied from 0 to 20 min to study the kinetics of oxidation. The oxidation process was characterized by atomic force microscopy (AFM) and micro-Raman spectroscopy.

Micro-Raman spectroscopy was used to characterize the overall structural change during the oxidation. The D peak at ~1350 cm^{-1} is an indicator of defects in graphene. Before any heat treatment, the D band in our single-layer graphene sample is barely detectable, indicating intrinsic defect concentration being very low. As shown in Figure 1a, after the sample was heated to 550 °C, the Raman spectra showed an increase in the intensity of D peak. No detectable morphology change was observed in the AFM image at this stage (Figure S1, also see discussions below), indicating that the disorder induced by oxidation is still at the atomic level. It was observed that the ratio of the intensity of D band to G band (I_D/I_G ratio) increased with the time of heating (Figure 1b). Upon thermal treatment, both G (~1580 cm^{-1}) and 2D (~2680 cm^{-1}) peaks shifted to significantly higher wavenumbers with a maximum G peak shift of ~16 cm^{-1}. This shift in the G and 2D peaks is consistent with hole-doping by oxygen.[14,41]

dx.doi.org/10.1021/jp306537y | J. Phys. Chem. C 2012, 116, 20600−20606

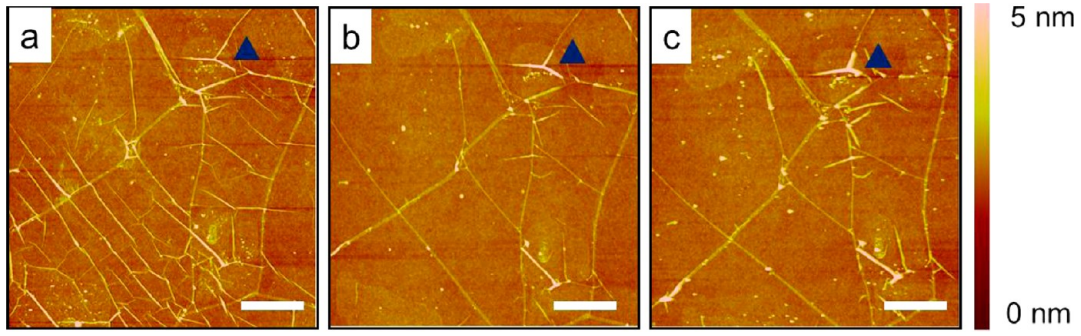

Figure 2. AFM images of CVD-grown single-layer graphene on Si/SiO_2 substrate (a) before, (b) after heating at 550 °C for 15 min under Ar/H_2, and (c) after heating at 550 °C for 45 min Ar/H_2. Scale bars represent 1 μm. All AFM images obtained at the same location. "▲" indicates the same location on the sample.

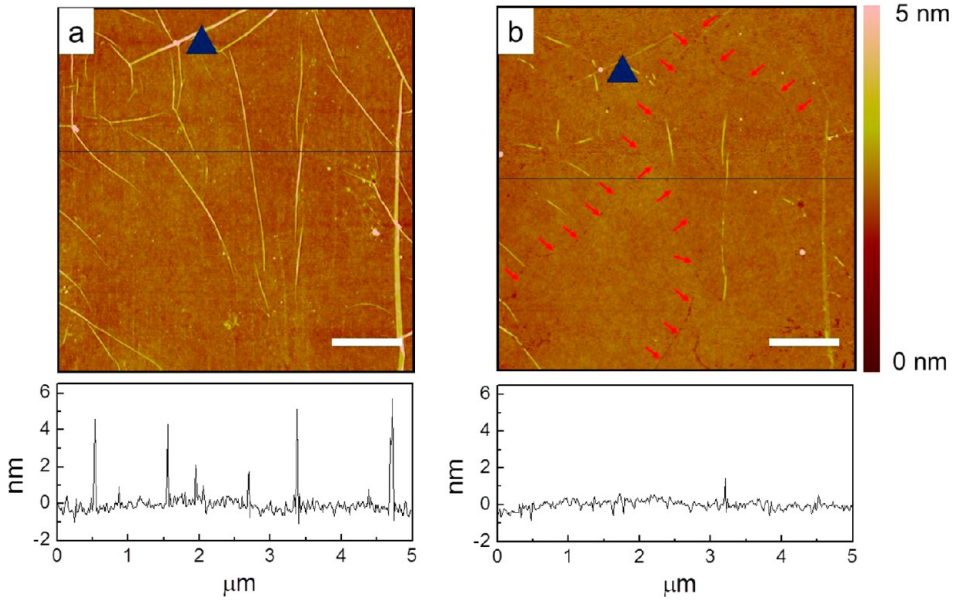

Figure 3. AFM images and cross sections of CVD-grown single-layer graphene on a Si/SiO_2 substrate (a) before and (b) after heating at 550 °C for 10 min in air. Scale bars represent 1 μm. "▲" indicates the same location on the sample. Red arrows indicate the cracks.

Figure 1c shows the AFM image of a single-layer graphene film after transferring to a Si/SiO_2 substrate but before oxidation. The graphene film has wrinkles of several micrometers in length and ~5−8 nm in height. The grain boundaries and point defects, however, are invisible to AFM. After 20 min of oxidation at 550 °C, we observed three significant changes in the surface morphology. First, most, if not all, of the wrinkles disappeared. Second, pits of ~20−100 nm in diameter appeared on the surface of graphene (Figure 1d). Similar nanoscale pits were observed in the oxidation of mechanically exfoliated graphene and were attributed to the preferential attack of point defects and the subsequently formed edges by oxygen;[14] we believe that a similar mechanism is in operation here. In addition to the pits, cracks of several tens of nanometer in width and up to several micrometers in length were also observed on the surface, suggesting a high density of defect sites within these regions. Similar cracks were observed in the oxidation of exfoliated graphene and were attributed to the oxidation of grain boundaries.[14] However, in our case, the cracks can originate from either the grain boundaries (atomic level defects) or the wrinkles (curved region, high strain).

We carried out a control experiment to separate the effect of thermal annealing from that of the O_2 oxidation. In this experiment, a graphene sample was heated under an Ar/H_2 atmosphere at the same temperature of the oxidation (550 °C). We used AFM to image the same location before and after the heating to characterize the change of morphology of graphene. Shown in Figure 2, we found that even after 40 min of heating, there were no cracks or pits observed on the graphene surface. Clearly, the formation of cracks and pits is entirely due to the oxidative etching of graphene, similar to the oxidation of exfoliated graphene and graphite.

The amount of wrinkles was significantly reduced by the high temperature annealing in Ar/H_2. However, not all wrinkles can be removed under this condition. Those wrinkles that did disappear did so within the first 15 min of the Ar/H_2 annealing (Figure 2b). Heating the sample for an additional 30 min under Ar/H_2 produced almost no change to the remaining wrinkles (Figure 2c). Qualitatively speaking, the wrinkles that survived the Ar/H_2 annealing (>3 μm) were typically longer than those that disappeared, although some isolated short wrinkles (<1 μm) did survive the annealing. In contrast, almost all wrinkles disappeared upon 20 min of heating at 550 °C in air (Figure 1d). These observations indicate that both the thermal annealing and the oxidative etching contribute to the disappearance of wrinkles.

dx.doi.org/10.1021/jp306537y | J. Phys. Chem. C 2012, 116, 20600−20606

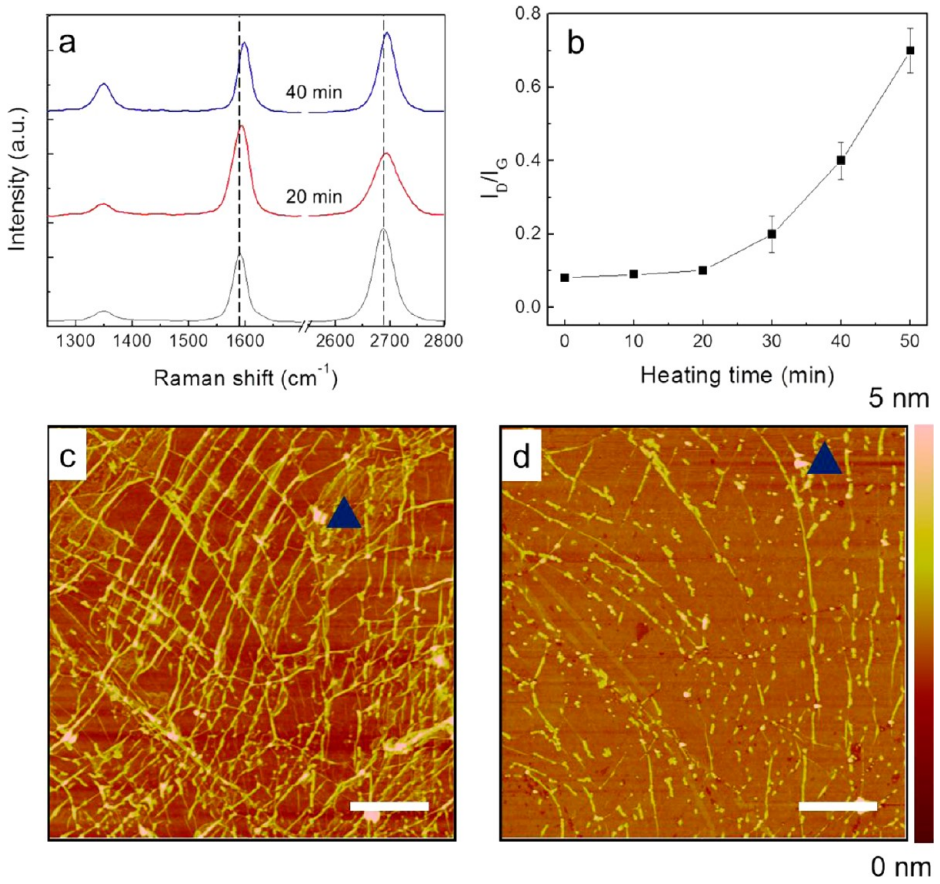

Figure 4. (a) Raman spectra of two-layer graphene on a Si/SiO_2 substrate before (black) and after heating at 550 °C for 20 min (red) and 40 min (blue). (b) Ratio of the intensity of G mode to D mode (I_D/I_G) as a function of heating time. The error bar is the standard deviation of 10 measurements taken at random locations. AFM images of two-layer graphene on Si/SiO_2 substrate (c) before and (d) after heating at 550 °C for 40 min in air. Scale bars represent 1 μm. "▲" indicates the same location of the sample.

To further elucidate the fate of the wrinkles and to determine the origin of the cracks formed in the oxidation, we repeated the oxidation experiment to capture the very early stage of the morphology change with AFM. Figure 3 shows two AFM images taken at the same location, one before and one after heating the sample in air at 550 °C for 10 min. The images clearly indicate that some of the wrinkles disappeared upon heating. The two line cross sections in Figure 3, taken at the same location, show a significant reduction in the height of the remaining wrinkles. Very narrow cracks (Figure 3b, red arrows) started to appear. Significantly, all of these cracks were located at previously wrinkle-free locations.

Our experiments showed that the wrinkles and cracks were not spatially correlated; the disappearance of wrinkles was not followed by the formation of cracks at the same location. This observation implies that the oxidation does not preferentially attack the wrinkles over the basal plane. We tentatively suggest that the cracks we observed in the oxidized graphene samples are likely due to the oxidative etching along grain boundaries instead of wrinkles. As we discussed, the wrinkles should have increased reactivity due to the high local curvature. However, whether the increased reactivity could be observed experimentally will largely depend on the magnitude of such increase, among many other factors. It is possible that the reactivity difference between the wrinkles and the basal plane is not significant enough to be observed under our reaction conditions.[42] Our graphene sample also contains a significant amount of point defects and grain boundaries, both of which showed significantly higher reactivity than wrinkles and basal plane. Finally, it is worth pointing out that some of the wrinkles disappeared within minutes of the thermal treatment (Figure S1). It is also possible that our failure to observe any increased reactivity on wrinkles may be due to their very short lifetime at high temperature.

Nevertheless, our experiments provided insight into the role of oxidation on the unwrinkling process. When heated in Ar/H_2, the unwrinkling process stopped before all of the wrinkles could disappear. In contrast, in the presence of O_2, all wrinkles disappeared from the graphene surface. Interestingly, even though O_2 oxidation enhances the removal of the wrinkles, this effect is not through the direct oxidative etching of wrinkles. One tentative explanation is that the nanoscale pits and cracks produced by the oxidation reduce the compressive stress within the graphene layer and weaken the interaction between graphene and the SiO_2 substrate. These two effects increase both the kinetics and the extent of the unwrinkling process. It is important to note that our study only probes the wrinkles visible to AFM. Graphene also has other types of microscopic structures (e.g., ripples) that are only observable by scanning tunneling microscopy (STM) or transmission electron microscopy (TEM).[43−45]

We have carried out the same oxidation experiment on two-layer graphene to evaluate the effect of thickness on the stability of graphene toward oxidation (Figure 4).[14] A previous study by Liu et al. showed that exfoliated graphene, presumably in A−B stacking order, is more stable than single-layer graphene toward

dx.doi.org/10.1021/jp306537y | J. Phys. Chem. C 2012, 116, 20600−20606

O_2 oxidation.[14] They proposed that the transition state of the oxidation involves an out-of-plane deformation of graphene. Single-layer graphene is more flexible than two-layer graphene and as a result shows an increased reactivity.

We prepared a two-layer graphene film by overlaying two CVD-grown single-layer graphene films on top of one another. Unlike exfoliated two-layer graphene, which exists in A−B stacking, our sample is almost certainly randomly stacked. The lack of stacking order in our sample can be seen in the Raman spectrum, where the 2D peak showed no apparent asymmetry, indicating the absence of well-defined electronic coupling between the two graphene layers (Figure 4a).[46] Our sample provides an opportunity to evaluate the role of stacking order on the reactivity of two-layer graphene.

We find that the two-layer graphene sample showed a much improved resistance to oxidation despite the absence of any stacking order. Upon oxidation, as shown in the Raman spectra (Figure 4a,b), the two-layer graphene sample showed a much slower buildup of D peak than did the single-layer sample. As observed in Figure 4b, even after 40 min of heating, the I_D/I_G ratio in two-layer graphene (I_D/I_G = ∼0.4) is much lower as compared to that of single-layer graphene after only 20 min of heating (I_D/I_G = ∼0.8, see Figure 1a,b). In addition, in the case of two-layer graphene, a significant increase in the D peak is observed only after 20 min of heating (Figure 4a,b), whereas in the case of single-layer graphene an increase in D peak is observed immediately after heating the sample to 550 °C (Figure 1a,b). Similar to the case of single-layer graphene, both G and 2D peaks in the two-layer graphene shifted to significantly higher wavenumbers, indicating doping of two-layer graphene by oxygen.

The same reactivity difference between single- and two-layer graphene was also observed in the AFM images. As shown in Figure 4c, the AFM image of the as-prepared two-layer graphene showed more wrinkles than did its single-layer counterpart. This is somewhat expected because the wrinkles from both layers are visible under AFM. As in the case of single-layer graphene, the unwrinkling effect was also observed upon heat treatment, although it occurred at a slower rate. We observed no significant pits or cracks after heating the two-layer graphene for 20 min at 550 °C (Figure S2). This observation is in contrast to the case of single-layer graphene, which developed a significant amount of pits and cracks under the same condition (Figure 1c,d). In the two-layer sample, nanoscale pits only started to appear after 40 min of oxidation (Figure 4d), clearly indicating a much lower reactivity toward oxidation than the single-layer graphene.

There are several reasons for the reduced reactivity in two-layer graphene. First, our result is consistent with the hypothesis that the increased stability in two-layer graphene is due to its higher stiffness than the single-layer sample.[14] Alternatively, the charged impurities in SiO_2 may also contribute to the observed reactivity difference. Recently, it was found that the charge impurities in SiO_2 are responsible for the increased electrochemical reactivity in single-layer graphene.[47] Given the electrochemical nature of the O_2 adsorption on graphene,[48] it is possible that the increased charge screening ability of the two-layer graphene could contribute to its enhanced stability toward oxidation. The third possibility is that only the top layer of the two-layer sample is reacting with oxygen, while the bottom layer is not. Graphene has been shown to form an airtight seal with a SiO_2 substrate.[49] It is possible that the bottom layer of a two-layer graphene is completely or partially inaccessible to O_2.

■ CONCLUSIONS

We have studied the thermal oxidation of CVD-grown single-layer and randomly stacked two-layer graphene. We find that the oxidation produced nanoscale pits and cracks in graphene, similar to the oxidation of exfoliated graphene and graphite. The single-layer graphene partially unwrinkled upon thermal annealing in Ar/H_2 at 550 °C and completely unwrinkled when heated in air. The thermal oxidation does not preferentially attack the wrinkles over the basal plane. Randomly stacked two-layer graphene shows increased resistance to oxidation as compared to single-layer graphene.

■ EXPERIMENTAL SECTION

Materials and Methods. All chemicals were used as purchased. Silicon wafer with a 300 nm thermal oxide layer was purchased from University Wafers. Tapping mode atomic force microscopy was carried out on a Veeco Dimension 3100. Raman spectrum was acquired on a home-built micro-Raman setup that consists of a 532 nm single-mode solid-state laser, a 532 nm cleanup filter (Semrock), an inverted microscope (Nikon Eclipse Ti/U), a long pass edge filter (Semrock), and a single stage spectrograph (Andor Shamrock 303, focal length: 303 mm) with an attached thermoelectric-cooled back-illuminated CCD camera (Andor iDus). A 40× objective (NA: 0.60) was used in all of the micro-Raman experiments. The laser power was kept below 2 mW in the micro-Raman experiments; control experiments showed that the laser-induced damage to the graphene sample is negligible.

CVD Synthesis of Graphene. Graphene was synthesized using a previously reported method.[9] In a typical procedure, a clean Cu foil (5 cm × 2 cm strips, cleaned by rinsing in concentrated HCl, DI water dried with N_2) was placed inside a 1 in. diameter quartz tube in a tube furnace. The tube was then evacuated, backfilled with hydrogen, and heated to 1000 °C under a H_2 flow (2 SCCM, SCCM: standard cubic centimeters per minute) and pressure of 70 mTorr. After annealing the Cu inside the furnace for 30 min (under H_2 flow), CH_4 (15 SCCM) was introduced into the furnace at a total pressure of 500 mTorr. After 30 min, the furnace was turned off and allowed to cool to room temperature under the H_2 and CH_4 gas flow.

Transfer of Graphene to a Si/SiO_2 Substrate (Single-Layer Graphene). The graphene film grown on the Cu catalyst surface was transferred to Si substrate using poly methyl-methacrylate (PMMA).[13] In a typical procedure, PMMA (50 mg/mL solution in anisole) was spin coated on the Cu foil containing graphene. Because graphene grows on both sides of the Cu, the graphene on the non PMMA-coated Cu surface was removed by placing the Cu foil in etching solution (1 M $FeCl_3$ in 10% HCl) for 2 min followed by a wipe with a Kimwipe. The PMMA/graphene/Cu foil was then placed again in the etching solution to etch away Cu. The floating PMMA/graphene film was transferred to a DI water bath to wash away etching impurities and was then collected onto a clean Si wafer and dried. A drop of PMMA solution was then placed on top of PMMA/graphene covering/wetting the entire surface and was left undisturbed for 30 min. It was then placed in an acetone bath overnight, followed by a dichloro-

dx.doi.org/10.1021/jp306537y | J. Phys. Chem. C 2012, 116, 20600−20606

methane bath for 8 h, and finally boiling in an acetone bath for 10 min to remove PMMA.

Preparation of Two-Layer Graphene. In a typical procedure, PMMA (50 mg/mL solution in anisole) was spin coated on the Cu foil containing graphene. Because graphene grows on both sides of the Cu foil, the graphene on the non PMMA-coated Cu surface was removed by placing the Cu foil in the etching solution (1 M $FeCl_3$ in 10% HCl) for 2 min followed by a wipe with a Kimwipe. The PMMA/graphene/Cu foil was then placed again in the etching solution to etch away the remaining Cu foil. The floating PMMA/graphene was transferred to a DI water bath to wash away etching impurities and was then collected onto another Cu foil containing graphene and dried to give a PMMA/graphene/graphene/Cu stack. Please note that the second Cu foil has graphene only on one side; the graphene on the other side was already removed using the etching solution following the above-described procedure. PMMA solution was spin coated on top of the PMMA/graphene/graphene/Cu stack and was then placed into the etching solution to etch away Cu. The floating film of PMMA/graphene/graphene was transferred to a DI water bath to wash away etching impurities and was then fished onto a clean Si wafer and dried. A drop of PMMA solution was then placed on top of PMMA/graphene/graphene covering the entire surface and was left undisturbed for 30 min. It was then placed in an acetone bath overnight, followed by a dichloromethane bath for 8 h, and finally boiling in an acetone bath for 10 min to dissolve PMMA, resulting in two-layer graphene onto Si substrate. The above process can be used for preparing as many graphene layers as one desires.

Thermal Treatment (Oxidation) of Graphene in Air. Graphene film transferred onto silicon substrate was placed inside an oven at room temperature and heated to 550 °C at the rate of 40 °C/min. Upon reaching 550 °C, the graphene sample was kept at that temperature for a fixed amount of time as indicated in the relevant figures and discussions.

Thermal Treatment of Graphene under Ar/H_2. Graphene film transferred onto silicon substrate was placed inside a tube furnace under a constant flow of argon (250 SCCM) and hydrogen (25 SCCM). The tube furnace was then heated to 550 °C at the rate of 50 °C/min. Upon reaching 550 °C, the graphene sample was kept at that temperature for a fixed amount of time as indicated in the relevant figures and discussions.

■ ASSOCIATED CONTENT

Supporting Information

Additional figures. This material is available free of charge via the Internet at http://pubs.acs.org.

■ AUTHOR INFORMATION

Corresponding Author

*E-mail: hliu@pitt.edu.

Notes

The authors declare no competing financial interest.

■ ACKNOWLEDGMENTS

We are thankful for financial support from the Mascaro Center for Sustainable Innovation and the Central Research Development Fund of University of Pittsburgh.

■ REFERENCES

(1) Geim, A. K. *Science* **2009**, *324*, 1530−1534.
(2) Geim, A. K.; Novoselov, K. S. *Nat. Mater.* **2007**, *6*, 183−191.
(3) Zhu, Y.; Murali, S.; Cai, W.; Li, X.; Suk, J. W.; Potts, J. R.; Ruoff, R. S. *Adv. Mater.* **2010**, *22*, 3906−3924.
(4) Allen, M. J.; Tung, V. C.; Kaner, R. B. *Chem. Rev.* **2010**, *110*, 132−145.
(5) Bae, S.; Kim, H.; Lee, Y.; Xu, X.; Park, J.-S.; Zheng, Y.; Balakrishnan, J.; Lei, T.; Kim, H. R.; Song, Y. I.; et al. *Nat. Nanotechnol.* **2010**, *5*, 574−578.
(6) Dua, V.; Surwade, S. P.; Ammu, S.; Agnihotra, S. R.; Jain, S.; Roberts, K. E.; Park, S.; Ruoff, R. S.; Manohar, S. K. *Angew. Chem., Int. Ed.* **2010**, *49*, 2154−2157.
(7) Robinson, J. T.; Perkins, F. K.; Snow, E. S.; Wei, Z.; Sheehan, P. E. *Nano Lett.* **2008**, *8*, 3137−3140.
(8) Wei, D.; Liu, Y. *Adv. Mater.* **2010**, *22*, 3225−3241.
(9) Li, X.; Cai, W.; An, J.; Kim, S.; Nah, J.; Yang, D.; Piner, R.; Velamakanni, A.; Jung, I.; Tutuc, E.; et al. *Science* **2009**, *324*, 1312−1314.
(10) Caldwell, J. D.; Anderson, T. J.; Culbertson, J. C.; Jernigan, G. G.; Hobart, K. D.; Kub, F. J.; Tadjer, M. J.; Tedesco, J. L.; Hite, J. K.; Mastro, M. A.; et al. *ACS Nano* **2010**, *4*, 1108−1114.
(11) Song, L.; Ci, L.; Gao, W.; Ajayan, P. M. *ACS Nano* **2009**, *3*, 1353−1356.
(12) Lee, Y.; Bae, S.; Jang, H.; Jang, S.; Zhu, S.-E.; Sim, S. H.; Song, Y. I.; Hong, B. H.; Ahn, J.-H. *Nano Lett.* **2010**, *10*, 490−493.
(13) Li, X.; Zhu, Y.; Cai, W.; Borysiak, M.; Han, B.; Chen, D.; Piner, R. D.; Colombo, L.; Ruoff, R. S. *Nano Lett.* **2009**, *9*, 4359−4363.
(14) Liu, L.; Ryu, S.; Tomasik, M. R.; Stolyarova, E.; Jung, N.; Hybertsen, M. S.; Steigerwald, M. L.; Brus, L. E.; Flynn, G. W. *Nano Lett.* **2008**, *8*, 1965−1970.
(15) Tao, H.; Moser, J.; Alzina, F.; Wang, Q.; Sotomayor-Torres, C. M. *J. Phys. Chem. C* **2011**, *115*, 18257−18260.
(16) Lee, G.; Lee, B.; Kim, J.; Cho, K. *J. Phys. Chem. C* **2009**, *113*, 14225−14229.
(17) Tracz, A.; Wegner, G.; Rabe, J. P. *Langmuir* **2003**, *19*, 6807−6812.
(18) Solis-Fernandez, P.; Paredes, J. I.; Cosio, A.; Martinez-Alonso, A.; Tascon, J. M. D. *J. Colloid Interface Sci.* **2010**, *344*, 451−459.
(19) Wang, X.; Dai, H. *Nat. Chem.* **2010**, *2*, 661−665.
(20) Kim, D. W.; Kim, Y. H.; Jeong, H. S.; Jung, H.-T. *Nat. Nanotechnol.* **2012**, *7*, 29−34.
(21) An, J.; Voelkl, E.; Suk, J. W.; Li, X.; Magnuson, C. W.; Fu, L.; Tiemeijer, P.; Bischoff, M.; Freitag, B.; Popova, E.; et al. *ACS Nano* **2011**, *5*, 2433−2439.
(22) Ogawa, Y.; Hu, B.; Orofeo, C. M.; Tsuji, M.; Ikeda, K.-i.; Mizuno, S.; Hibino, H.; Ago, H. *J. Phys. Chem. Lett.* **2012**, *3*, 219−226.
(23) Gao, L.; Guest Jeffrey, R.; Guisinger Nathan, P. *Nano Lett* **2010**, *10*, 3512−6.
(24) Kim, K.; Lee, Z.; Regan, W.; Kisielowski, C.; Crommie, M. F.; Zettl, A. *ACS Nano* **2011**, *5*, 2142−2146.
(25) Li, X.; Magnuson Carl, W.; Venugopal, A.; An, J.; Suk, J. W.; Han, B.; Borysiak, M.; Cai, W.; Velamakanni, A.; Zhu, Y.; et al. *Nano Lett.* **2010**, *10*, 4328−34.
(26) Huang, P. Y.; Ruiz-Vargas, C. S.; van der Zande, A. M.; Whitney, W. S.; Levendorf, M. P.; Kevek, J. W.; Garg, S.; Alden, J. S.; Hustedt, C. J.; Zhu, Y.; et al. *Nature* **2011**, *469*, 389−392.
(27) Yu, Q. K.; Jauregui, L. A.; Wu, W.; Colby, R.; Tian, J. F.; Su, Z. H.; Cao, H. L.; Liu, Z. H.; Pandey, D.; Wei, D. G.; et al. *Nat. Mater.* **2011**, *10*, 443−449.
(28) Liu, Y.; Yakobson, B. I. *Nano Lett.* **2010**, *10*, 2178−2183.
(29) Wang, B.; Puzyrev, Y.; Pantelides, S. T. *Carbon* **2011**, *49*, 3983−3988.
(30) Xu, S. C.; Irle, S.; Musaev, D. G.; Lin, M. C. *J. Phys. Chem. C* **2007**, *111*, 1355−1365.
(31) Jiang, D.-e.; Sumpter, B. G.; Dai, S. *J. Chem. Phys.* **2007**, *126*, 134701/1−134701/6.

(32) Nemes-Incze, P.; Yoo, K. J.; Tapaszto, L.; Dobrik, G.; Labar, J.; Horvath, Z. E.; Hwang, C.; Biro, L. P. *Appl. Phys. Lett.* **2011**, *99*, 023104.
(33) Yang, R.; Zhang, L. C.; Wang, Y.; Shi, Z. W.; Shi, D. X.; Gao, H. J.; Wang, E. G.; Zhang, G. Y. *Adv. Mater.* **2010**, *22*, 4014−4019.
(34) Liu, N.; Pan, Z. H.; Fu, L.; Zhang, C. H.; Dai, B. Y.; Liu, Z. F. *Nano Res.* **2011**, *4*, 996−1004.
(35) Zhu, W.; Low, T.; Perebeinos, V.; Bol, A. A.; Zhu, Y.; Yan, H.; Tersoff, J.; Avouris, P. *Nano Lett.* **2012**, *12*, 3431−3436.
(36) Yudasaka, M.; Zhang, M.; Iijima, S. *Chem. Phys. Lett.* **2003**, *374*, 132−136.
(37) Zhou, W.; Ooi, Y. H.; Russo, R.; Papanek, P.; Luzzi, D. E.; Fischer, J. E.; Bronikowski, M. J.; Willis, P. A.; Smalley, R. E. *Chem. Phys. Lett.* **2001**, *350*, 6−14.
(38) Starodub, E.; Bartelt, N. C.; McCarty, K. F. *J. Phys. Chem. C* **2010**, *114*, 5134−5140.
(39) Han, T.-H.; Huang, Y.-K.; Tan, A. T. L.; Dravid, V. P.; Huang, J.-X. *J. Am. Chem. Soc.* **2011**, *133*, 15264−15267.
(40) Zhao, S.; Surwade Sumedh, P.; Li, Z.; Liu, H. *Nanotechnology* **2012**, *23*, 355703.
(41) Ryu, S.-M.; Liu, L.; Berciaud, S.; Yu, Y.-J.; Liu, H.-T.; Kim, P.; Flynn, G. W.; Brus, L. E. *Nano Lett.* **2010**, *10*, 4944−4951.
(42) Luo, J.; Jang, H. D.; Sun, T.; Xiao, L.; He, Z.; Katsoulidis, A. P.; Kanatzidis, M. G.; Gibson, J. M.; Huang, J. *ACS Nano* **2011**, *5*, 8943−8949.
(43) de Parga, A. L. V.; Calleja, F.; Borca, B.; Passeggi, M. C. G.; Hinarejos, J. J.; Guinea, F.; Miranda, R. *Phys. Rev. Lett.* **2008**, *100*, 056807/1−056807/4.
(44) Fasolino, A.; Los, J. H.; Katsnelson, M. I. *Nat. Mater.* **2007**, *6*, 858−861.
(45) Meyer, J. C.; Geim, A. K.; Katsnelson, M. I.; Novoselov, K. S.; Booth, T. J.; Roth, S. *Nature* **2007**, *446*, 60−63.
(46) Ferrari, A. C.; Meyer, J. C.; Scardaci, V.; Casiraghi, C.; Lazzeri, M.; Mauri, F.; Piscanec, S.; Jiang, D.; Novoselov, K. S.; Roth, S.; et al. *Phys. Rev. Lett.* **2006**, *97*, 187401/1−187401/4.
(47) Sharma, R.; Baik, J. H.; Perera, C. J.; Strano, M. S. *Nano Lett.* **2010**, *10*, 398−405.
(48) Sato, Y.; Takai, K.; Enoki, T. *Nano Lett.* **2011**, *11*, 3468−3475.
(49) Koenig, S. P.; Boddeti, N. G.; Dunn, M. L.; Bunch, J. S. *Nat. Nanotechnol.* **2011**, *6*, 543−546.